is proposed that ribavirin inhibits the RNA capping and RNA polymerization by virus-encoded enzymes [40]. It is also known that since ribavirin forms hydrogen bonds with cytidine and uridine, the incorporation of ribavirin into viral genomic RNA induces G to A transition leading to the lethal mutations [29].

In this study, to elucidate functional residues required for the PB1 activity, we tried to isolate PB1 mutants which are resistant to ribavirin. We found that the amino acid position 27 of PB1 is important for nucleotide recognition.

2. Materials and methods

2.1. Biological materials

Monolayer cultures of 293T and MDCK cells were maintained at 37 °C in Dulbecco's Modified Eagle Medium (DMEM) and minimal essential medium (MEM) (Nissui), respectively, supplemented with 10% fetal bovine serum (Bovogen). Influenza virus strain A/WSN/33 was prepared as previously described [8]. Ribavirin (Sigma) was dissolved in water to make stock of 100 μM.

2.2. PB1 random mutagenesis

For construction of a mammalian expression vector for PB1 containing random mutations, we used a PCR-based cloning strategy in the presence of $MnCl_2$. cDNA corresponding to the full-length PB1 was amplified with specific primers 5′-CCCCAAGCTTGCCGCC ACCATGGATGTCAATCCGACCTT-3′ and 5′-CATGCGGCCGCCTATTT TTGCCGTCTGAGCTCTT-3′. The PCR product was then cloned into the *Hind* III and *Not* I sites of pEGFP-N1 and replaced *EGFP* gene with mutated *PB1* cDNA. The mutation rate of the plasmid library was confirmed by sequencing randomly selected 20 clones using specific primer 5′-GGAAGGCTCATAGACTTCCTTA-3′, which is corresponding to the nucleotide position from 560 to 1050 of segment 2. The plasmid library was then used to analyze the influenza virus RNA polymerase activity in a mini-replicon assay system.

2.3. Mini-replicon assay system

293T cells were transfected with plasmids for the expression of viral proteins, PB1 (wild-type or mutants), PB2, PA, and NP, and a plasmid for the expression of artificial influenza virus genome containing either *EGFP* gene (for screening) or the *firely luciferase* gene (for luciferase assay) of negative polarity, which is synthesized in cells by the human DNA-dependent RNA polymerase I [41]. The mRNAs encoding either *EGFP* or *luciferase* genes are transcribed in a viral RNA polymerase-dependent manner. For the screening, ribavirin was added (0 or 75 μM) after 3 h post transfection (hpt), and the fluorescence of EGFP was observed at 15 hpt. For the luciferase assay, ribavirin was added in the medium at various concentrations after 3 hpt, incubated at 37 °C for 15 h, and then the luciferase activity was determined using commercially available reagents (Promega) according to the manufacturer's protocol. The relative luminescence intensity was measured with a luminometer for 20 s. A plasmid for the expression of *Renilla* luciferase driven by the simian virus 40 (SV40) promoter was used as an internal control for the dual-luciferase assay. As a negative control, 293T cells were transfected with the same plasmids, except for the PB1 expression plasmid.

3. Results

3.1. Screening of ribavirin-resistant PB1 mutants

To determine the 50% inhibitory concentration (IC_{50}) of ribavirin, we carried out plaque assays with WSN-infected MDCK cells in the presence of various concentrations of ribavirin (Fig. 1A). Based on the results, we determined that IC_{50} and IC_{90} of ribavirin on influenza virus were 20 and 75 μM, respectively.

To make mutated cDNA library of PB1, random mutagenesis was carried out by PCR in the presence of 0.1 mM of Mn^{2+} and 1.5 mM of Mg^{2+} as described in Section 2. To know the mutation frequency of this library, we transformed the library into *Escherichia coli* DH5α high competent cells and obtained 3×10^4 colonies. To evaluate the mutation frequency, plasmids were isolated from 20 independent colonies and sequenced between the nucleotide positions 560 and 1055 of *PB1* gene. The results of sequencing showed that approximately 4.7 mutations were introduced in 2,274 nucleotides of *PB1* gene on average (approximately 1–2 a.a./PB1 protein). Based on this in hand, we started screening of ribavirin-resistant PB1 from the mutated cDNA library as shown in Fig. 1B. At first, this library was divided into 10 groups (Group 1–10), and mini-replicon assays were performed in the presence of ribavirin at IC_{90} (Fig. 1C), and thereby EGFP-positive cells were hardly found in wild-type PB1 transfected cells. In contrast, in the case of cDNA library-transfected cells, approximately 10–30% of EGFP-positive cells were found. Among them, 34% of one of groups, Group 4-transfected cells were resistant to ribavirin on average. Thus, Group 4 was further divided into additional 10 groups and subjected to the mini-replicon assays. After enrichment by 5 time-repetitions of this cycle, we could isolate a single clone showing the resistance to ribavirin. Even in the presence of IC_{90} of ribavirin, 69% of the isolated clone-transfected cells were EGFP positive (Fig. 2A). By sequencing of the isolated clone, we found one nucleotide substitution from G to A at nucleotide position of 103 (where the 5′ terminal nucleotide of cRNA is referred to as nucleotide position 1). This nucleotide change leads to an amino acid change from Asp to Asn at amino acid position 27 (Fig. 2B).

3.2. Characterization of D27N mutant

To quantitatively measure the influenza virus RNA polymerase activity, the mini-replicon assays with the artificial genome containing *luciferase* gene was carried out in the presence of 12.5, 25, and 50 μM of ribavirin, respectively. The luciferase activity of D27N mutant remained even in the presence of ribavirin compared with that of wild type. IC_{50} of D27N to ribavirin was about 18 μM, while that of wild-type was around 10 μM (Fig. 2C). Furthermore, the expression level of D27N was confirmed by Western blot analysis. The expression level of D27N was unchanged compared with that of wild-type even in the absence or presence of 50 μM ribavirin (Fig. 2D).

To further characterize this mutant, we used methotrexate (MTX). MTX is an inhibitor for purine biosynthesis, resulting in decrease of intracellular purine concentration. The mini-replicon assays were performed in the presence of various concentrations of MTX. The viral polymerase activity of D27N was significantly more than that of wild-type even in the presence of MTX (Fig. 3).

4. Discussion

PB1 functions as a catalytic subunit of viral RNA polymerase [2–7] and contains the highly conserved motifs of RNA-dependent RNA polymerases [2]. Putative nucleotide-binding sites have been expected adjacent to the conserved motifs of RNA-dependent RNA polymerases [23,24]. PB1 also binds to the vRNA and cRNA promoters [25,27]. In this study, to elucidate the functional domain of PB1 involved in nucleotide recognition, we isolated ribavirin-resistant mutants. Ribavirin inhibits the *de novo* synthesis of purine nucleosides and thus blocks viral RNA synthesis. In addition, it has been proposed that ribavirin also inhibits directly the

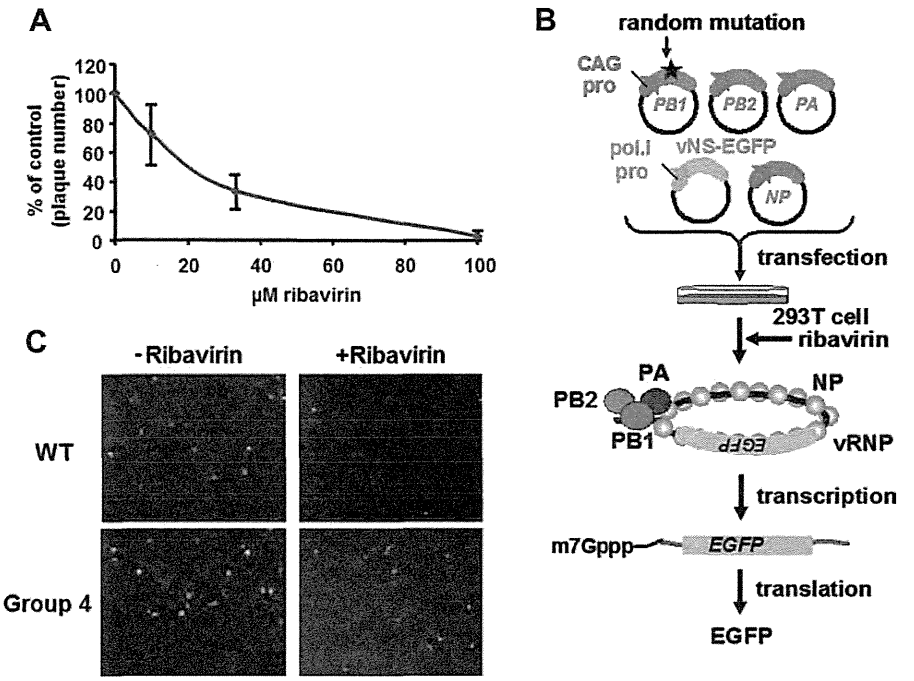

Fig. 1. Screening of ribavirin-resistant PB1 mutant. (A) Plaque assays were carried out with MDCK cells-infected WSN at MOI of 0.25×10^{-4} in the presence of ribavirin (0, 10, 33, 100, and 300 μM). The results are averages from three independent experiments with standard deviations. (B) Assay system for screening by mini-replicon assay. 293T cells were transfected with plasmids for the expression of viral proteins, PB1 (wild-type or mutant), PB2, PA, and NP, and a plasmid for the expression of artificial influenza virus genome containing *EGFP* gene of negative polarity. (C) At 3 hpt, ribavirin was added (0 or 75 μM), and the fluorescence of EGFP was observed at 15 hpt.

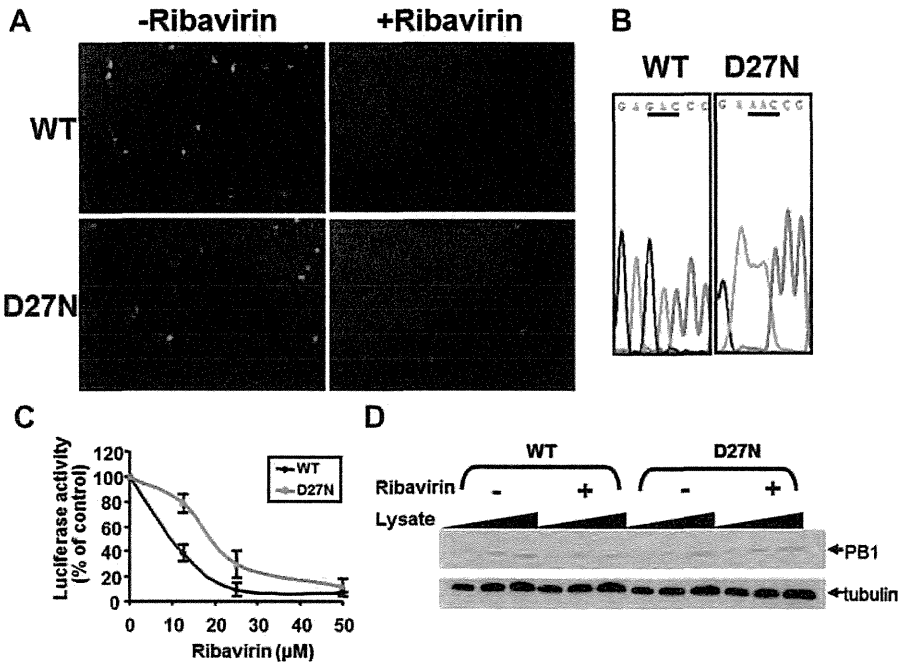

Fig. 2. Ribavirin-resistance of D27N mutant by mini-replicon assay system. (A) Mini-replicon assay using *EGFP* gene as a reporter gene. At 3 hpt, ribavirin was added (0 or 75 μM), and the fluorescence of EGFP was observed at 15 hpt. (B) Sequence of ribavirin-resistant PB1 mutant. (C) Mini-replicon assay using *luciferase* gene as a reporter gene was carried out. At 3 hpt, different concentrations (0, 12.5, 25, 50, and 100 μM) of ribavirin were added, and the luciferase activity was measured at 15 hpt. The vertical axis represents the percentage of the luciferase activity from ribavirin-treated cells relative to that from ribavirin-untreated cells. The results are averages from three independent experiments with standard deviations. (D) Effect of D27N mutation on assembly of PB1 subunit. Mini-replicon assay using *luciferase* gene as a reporter gene was carried out. At 3 hpt, ribavirin was added (0 or 50 μM). At 15 hpt, cells were lysed, and the lysates were subjected to Western blot analysis using anti-PB1 antibody and antibody against β-tubulin.

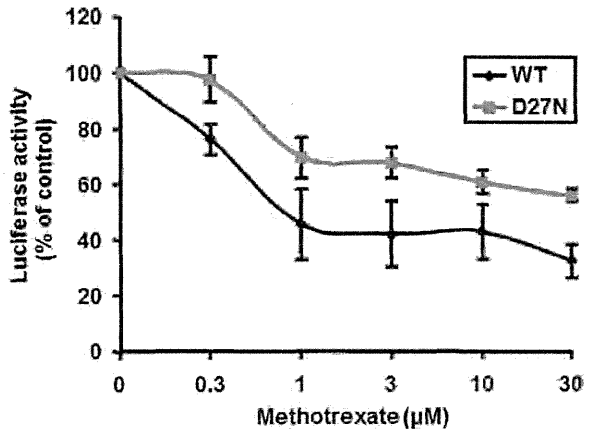

Fig. 3. Methotrexate-resistance of D27N mutant by mini-replicon assay system. The mini-replicon assay using *luciferase* gene as a reporter gene was carried out. At 12 hpt, different concentrations (0, 0.3, 1, 3, 10, and 30 μM) of methotrexate were added, and luciferase activity was measured at 22 hpt. The vertical axis represents the percentage of the luciferase activity from methotrexate-treated cells relative to that from methotrexate-untreated cells. The results are averages from three independent experiments with standard deviations.

viral RNA synthesis. We found that the viral polymerase activity of D27N was higher than that of wild type in the presence of ribavirin (Fig. 2C). Further, the viral polymerase activity of D27N was also resistant to MTX treatment compared with that of wild type (Fig. 3). These strongly suggest that D27 N mutant can polymerize the nascent RNA chains with the low concentrations of nucleotide. Therefore, it is expected that Asp27 is involved in the nucleotide recognition.

The Asp27 of PB1 is conserved over 99.9% of 7259 sequences of PB1 deposited in the NCBI Influenza Sequence Database. It has been reported that Asp27 is located upstream of the nucleotide binding site of PB1 but not in the catalytic active site. Similarly, the ribavirin-resistant mutant of poliovirus has a mutation in a domain out of the catalytic active site of the viral polymerase [42]. D27N is present within putative vRNA and cRNA promoter binding sites [25,27]. It is shown by mutants in the promoters of vRNA and cRNA that the RNA synthesis activity, cleavage of the cap structure, and the polyadenylation by viral polymerase are regulated through the promoter structure [43–45]. Further, the viral polymerase is stabilized by the interaction with its viral promoter [46]. Based on previous reports and our findings, the interaction between Asp27 of PB1 with vRNA and/or cRNA promoters may lead to the regulation of viral polymerase activity through the nucleotide recognition activity of PB1. This finding could useful for further studies about the mechanism of nucleotide recognition of the influenza viral RNA polymerase.

Acknowledgments

This research was supported in part by Grants-in-aid from the Ministry of Education, Culture, Sports, Science, and Technology of Japan (to K.N.).

References

[1] M.-L. Li, P. Rao, R.M. Krug, The active sites of the influenza cap-dependent endonuclease are on different polymerase subunits, EMBO J. 20 (2001) 2078–2086.
[2] S.K. Biswas, D.P. Nayak, Mutational analysis of the conserved motifs of influenza A virus polymerase basic protein 1, J. Virol. 68 (1994) 1819–1826.
[3] S.K. Biswas, D.P. Nayak, Influenza virus polymerase basic protein 1 interacts with influenza virus polymerase basic protein 2 at multiple sites, J. Virol. 70 (1996) 6716–6722.
[4] S. González, T. Zürcher, J. Ortín, Identification of two separate domains in the influenza virus PB1 protein involved in the interaction with the PB2 and PA subunits: a model for the viral RNA polymerase structure, Nucleic Acids Res. 24 (1996) 4456–4463.
[5] Y. Ohtsu, Y. Honda, T. Toyoda, Fine mapping of the subunit binding sites of influenza virus RNA polymerase, Int. Congr. Ser. 1219 (2001) 463–469.
[6] T. Toyoda, D.M. Adyshev, M. Kobayashi, A. Iwata, A. Ishihama, Molecular assembly of the influenza virus RNA Polymerase: determination of the subunit-subunit contact sites, J. Gen. Virol. 77 (1996) 2149–2157.
[7] T. Zürcher, S. de la Luna, J.J. Sanz-Ezquerro, A. Nieto, J. Ortín, Mutational analysis of the influenza virus A/Victoria/3/75 PA protein: studies of interaction with PB1 protein and identification of a dominant negative mutant, J. Gen. Virol. 77 (Pt. 8) (1996) 1745–1749.
[8] A. Kawaguchi, T. Naito, K. Nagata, Involvement of influenza virus PA subunit in assembly of functional RNA polymerase complexes, J. Virol. 79 (2005) 732–744.
[9] A. Dias, D. Bouvier, T. Crepin, A.A. McCarthy, D.J. Hart, F. Baudin, S. Cusack, R.W.H. Ruigrok, The cap-snatching endonuclease of influenza virus polymerase resides in the PA subunit, Nature 458 (2009) 914–918.
[10] E. Fodor, M. Crow, L.J. Mingay, T. Deng, J. Sharps, P. Fechter, G.G. Brownlee, A single amino acid mutation in the PA subunit of the influenza virus RNA polymerase inhibits endonucleolytic cleavage of capped RNAs, J. Virol. 76 (2002) 8989–9001.
[11] K. Hara, F.I. Schmidt, M. Crow, G.G. Brownlee, Amino acid residues in the N-terminal region of the PA subunit of influenza A virus RNA polymerase play a critical role in protein stability, endonuclease activity, cap binding, and virion RNA promoter binding, J. Virol. 80 (2006) 7789–7798.
[12] P. Yuan, M. Bartlam, Z. Lou, S. Chen, J. Zhou, X. He, Z. Lv, R. Ge, X. Li, T. Deng, E. Fodor, Z. Rao, Y. Liu, Crystal structure of an avian influenza polymerase PAN reveals an endonuclease active site, Nature 458 (2009) 909–913.
[13] P. Fechter, L. Mingay, J. Sharps, A. Chambers, E. Fodor, G.G. Brownlee, Two aromatic residues in the PB2 subunit of influenza A RNA polymerase are crucial for cap binding, J. Biol. Chem. 278 (2003) 20381–20388.
[14] D. Guilligay, F. Tarendeau, P. Resa-Infante, R. Coloma, T. Crepin, P. Sehr, J. Lewis, R.W.H. Ruigrok, J. Ortin, D.J. Hart, S. Cusack, The structural basis for cap binding by influenza virus polymerase subunit PB2, Nat. Struct. Mol. Biol. 15 (2008) 500–506.
[15] S.J. Plotch, M. Bouloy, I. Ulmanen, R.M. Krug, A unique cap(m7G pppXm)-dependent influenza virion endonuclease cleaves capped RNAs to generate the primers that initiate viral RNA transcription, Cell 23 (1981) 847–858.
[16] C. Wakai, M. Iwama, K. Mizumoto, K. Nagata, Recognition of cap structure by influenza B virus RNA polymerase is less dependent on the methyl residue than recognition by influenza A virus polymerase, J. Virol. 85 (2011) 7504–7512.
[17] A. Ghanem, D. Mayer, G. Chase, W. Tegge, R. Frank, G. Kochs, A. GarcÃ-a-Sastre, M. Schwemmle, Peptide-mediated interference with influenza A virus polymerase, J. Virol. 81 (2007) 7801–7804.
[18] D.R. Pérez, R.O. Donis, A 48-amino-acid region of influenza A virus PB1 protein is sufficient for complex formation with PA, J. Virol. 69 (1995) 6932–6939.
[19] E. Obayashi, H. Yoshida, F. Kawai, N. Shibayama, A. Kawaguchi, K. Nagata, J.R. Tame, S.Y. Park, The structural basis for an essential subunit interaction in influenza virus RNA polymerase, Nature 454 (2008) 1127–1131.
[20] X. He, J. Zhou, M. Bartlam, R. Zhang, J. Ma, Z. Lou, X. Li, J. Li, A. Joachimiak, Z. Zeng, R. Ge, Z. Rao, Y. Liu, Crystal structure of the polymerase PAC–PB1N complex from an avian influenza H5N1 virus, Nature 454 (2008) 1123–1126.
[21] E.L. Poole, L. Medcalf, D. Elton, P. Digard, Evidence that the C-terminal PB2-binding region of the influenza A virus PB1 protein is a discrete Î±-helical domain, FEBS Lett. 581 (2007) 5300–5306.
[22] K. Sugiyama, E. Obayashi, A. Kawaguchi, Y. Suzuki, J.R.H. Tame, K. Nagata, S.-Y. Park, Structural insight into the essential PB1–PB2 subunit contact of the influenza virus RNA polymerase, EMBO J. 28 (2009) 1803–1811.
[23] Y. Asano, A. Ishihama, Identification of two nucleotide-binding domains on the PB1 subunit of influenza virus RNA polymerase, J. Biochem. 122 (1997) 627–634.
[24] D.M. Kolpashchikov, A. Honda, A. Ishihama, Structure-function relationship of the influenza virus RNA polymerase: primer-binding site on the PB1 subunit, Biochemistry 43 (2004) 5882–5887.
[25] S. Gonzalez, J. Ortin, Characterization of influenza virus PB1 protein binding to viral RNA: two separate regions of the protein contribute to the interaction domain, J. Virol. 73 (1999) 631–637.
[26] M.-L. Li, B.C. Ramirez, R.M. Krug, RNA-dependent activation of primer RNA production by influenza virus polymerase: different regions of the same protein subunit constitute the two required RNA-binding sites, EMBO J. 17 (1998) 5844–5852.
[27] S. Gonzalez, J. Ortin, Distinct regions of influenza virus PB1 polymerase subunit recognize vRNA and cRNA templates, EMBO J. 18 (1999) 3767–3775.
[28] R.W. Sidwell, J.H. Huffman, G.P. Khare, L.B. Allen, J.T. Witkowski, R.K. Robins, Broad-spectrum antiviral activity of virazole: 1-β-D-ribofuranosyl-1,2,4-triazole-3-carboxamide, Science 177 (1972) 705–706.
[29] N.M. Dixit, A.S. Perelson, The metabolism, pharmacokinetics and mechanisms of antiviral activity of ribavirin against hepatitis C virus, Cell. Mol. Life Sci. 63 (2006) 832–842.
[30] J.J. Feld, J.H. Hoofnagle, Mechanism of action of interferon and ribavirin in treatment of hepatitis C, Nature 436 (2005) 967–972.
[31] B. Eriksson, E. Helgstrand, N.G. Johansson, A. Larsson, A. Misiorny, J.O. Noren, L. Philipson, K. Stenberg, G. Stening, S. Stridh, B. Oberg, Inhibition of influenza virus ribonucleic acid polymerase by ribavirin triphosphate, Antimicrob. Agents Chemother. 11 (1977) 946–951.

[32] P. Toltzis, K. O'Connell, J.L. Patterson, Effect of phosphorylated ribavirin on vesicular stomatitis virus transcription, Antimicrob. Agents Chemother. 32 (1988) 492–497.
[33] L.F. Cassidy, J.L. Patterson, Mechanism of La Crosse virus inhibition by ribavirin, Antimicrob. Agents Chemother. 33 (1989) 2009–2011.
[34] Y. Sun, D.-H. Chung, Y.-K. Chu, C.B. Jonsson, W.B. Parker, Activity of ribavirin against Hantaan Virus correlates with production of ribavirin-5′-triphosphate, not with inhibition of IMP dehydrogenase, Antimicrob. Agents Chemother. 51 (2007) 84–88.
[35] C.-y. Zheng, Chao-jiang Gu, Qian Zhang, Li-li Shi, Yong Li, San-fu Qu, An antiviral mechanism investigated with ribavirin as an RNA virus mutagen for foot-and-mouth disease virus, Biochem. Mol. Biol. 39 (2006) 9–15.
[36] I. Jordan, T. Briese, N. Fischer, J.Y.-N. Lau, W.I. Lipkin, Ribavirin inhibits west Nile virus replication and cytopathic effect in neural cells, J. Infect. Dis. 182 (2000) 1214–1217.
[37] D. Safronetz, E. Haddock, F. Feldmann, H. Ebihara, H. Feldmann, In vitro and in vivo activity of ribavirin against Andes virus infection, PLoS One 6 (2011) e23560.
[38] D. Maag, C. Castro, Z. Hong, C.E. Cameron, Hepatitis C virus RNA-dependent RNA polymerase (NS5B) as a mediator of the antiviral activity of ribavirin, J. Biol. Chem. 276 (2001) 46094–46098.
[39] W.E. Müller, A. Maidhof, H. Taschner, R.K. Zahn, Virazole (1-beta-D-ribofuranosyl-1,2,4-triazole-3-carboxamide; a cytostatic agent, Biochem. Pharmacol. 26 (1977) 1071–1075.
[40] J.D. Graci, C.E. Cameron, Mechanisms of action of ribavirin against distinct viruses, Rev. Med. Virol. 16 (2006) 37–48.
[41] K. Turan, M. Mibayashi, K. Sugiyama, S. Saito, A. Numajiri, K. Nagata, Nuclear MxA proteins form a complex with influenza virus NP and inhibit the transcription of the engineered influenza virus genome, Nucleic Acids Res. 32 (2004) 643–652.
[42] J.K. Pfeiffer, K. Kirkegaard, A single mutation in poliovirus RNA-dependent RNA polymerase confers resistance to mutagenic nucleotide analogs via increased fidelity, Proc. Natl. Acad. Sci. USA 100 (2003) 7289–7294.
[43] L.L.M. Poon, D.C. Pritlove, E. Fodor, G.G. Brownlee, Direct evidence that the poly (A) tail of influenza A virus mRNA is synthesized by reiterative copying of a U track in the virion RNA template, J. Virol. 73 (1999) 3473–3476.
[44] M.B. Leahy, G. Zecchin, G.G. Brownlee, Differential activation of influenza A virus endonuclease activity is dependent on multiple sequence differences between the virion RNA and cRNA promoters, J. Virol. 76 (2002) 2019–2023.
[45] M. Crow, T. Deng, M. Addley, G.G. Brownlee, Mutational analysis of the influenza virus cRNA promoter and identification of nucleotides critical for replication, J. Virol. 78 (2004) 6263–6270.
[46] G.G. Brownlee, J.L. Sharps, The RNA polymerase of influenza A virus is stabilized by interaction with its viral RNA promoter, J. Virol. 76 (2002) 7103–7113.

JVI Journals.ASM.org

The Host Protease TMPRSS2 Plays a Major Role in *In Vivo* Replication of Emerging H7N9 and Seasonal Influenza Viruses

Kouji Sakai,[a] Yasushi Ami,[b] Maino Tahara,[a] Toru Kubota,[a] Masaki Anraku,[a] Masako Abe,[a] Noriko Nakajima,[c] Tsuyoshi Sekizuka,[d] Kazuya Shirato,[a] Yuriko Suzaki,[b] Akira Ainai,[e] Yuichiro Nakatsu,[a] Kazuhiko Kanou,[f] Kazuya Nakamura,[e] Tadaki Suzuki,[c] Katsuhiro Komase,[a] Eri Nobusawa,[e] Katsumi Maenaka,[g] Makoto Kuroda,[d] Hideki Hasegawa,[c] Yoshihiro Kawaoka,[h,i,j] Masato Tashiro,[e] Makoto Takeda[a]

Department of Virology 3,[a] Division of Experimental Animal Research,[b] and Influenza Virus Research Center,[e] National Institute of Infectious Diseases, Tokyo, Japan; Department of Pathology,[c] Laboratory of Bacterial Genomics, Pathogen Genomics Center,[d] and Infectious Disease Surveillance Center,[f] National Institute of Infectious Diseases, Tokyo, Japan; Laboratory of Biomolecular Science, Faculty of Pharmaceutical Sciences, Hokkaido University, Hokkaido, Japan[g]; Division of Virology, Department of Microbiology and Immunology, and International Research Center for Infectious Diseases, Institute of Medical Science, The University of Tokyo, Tokyo, Japan[h]; ERATO Infection-Induced Host Responses Project, Japan Science and Technology Agency, Saitama, Japan[i]; Influenza Research Institute, University of Wisconsin—Madison, Madison, Wisconsin, USA[j]

ABSTRACT

Proteolytic cleavage of the hemagglutinin (HA) protein is essential for influenza A virus (IAV) to acquire infectivity. This process is mediated by a host cell protease(s) *in vivo*. The type II transmembrane serine protease TMPRSS2 is expressed in the respiratory tract and is capable of activating a variety of respiratory viruses, including low-pathogenic (LP) IAVs possessing a single arginine residue at the cleavage site. Here we show that TMPRSS2 plays an essential role in the proteolytic activation of LP IAVs, including a recently emerged H7N9 subtype, *in vivo*. We generated TMPRSS2 knockout (KO) mice. The TMPRSS2 KO mice showed normal reproduction, development, and growth phenotypes. In TMPRSS2 KO mice infected with LP IAVs, cleavage of HA was severely impaired, and consequently, the majority of LP IAV progeny particles failed to gain infectivity, while the viruses were fully activated proteolytically in TMPRSS2$^{+/+}$ wild-type (WT) mice. Accordingly, in contrast to WT mice, TMPRSS2 KO mice were highly tolerant of challenge infection by LP IAVs (H1N1, H3N2, and H7N9) with ≥1,000 50% lethal doses (LD_{50}) for WT mice. On the other hand, a high-pathogenic H5N1 subtype IAV possessing a multibasic cleavage site was successfully activated in the lungs of TMPRSS2 KO mice and killed these mice, as observed for WT mice. Our results demonstrate that recently emerged H7N9 as well as seasonal IAVs mainly use the specific protease TMPRSS2 for HA cleavage *in vivo* and, thus, that TMPRSS2 expression is essential for IAV replication *in vivo*.

IMPORTANCE

Influenza A virus (IAV) is a leading pathogen that infects and kills many humans every year. We clarified that the infectivity and pathogenicity of IAVs, including a recently emerged H7N9 subtype, are determined primarily by a host protease, TMPRSS2. Our data showed that TMPRSS2 is the key host protease that activates IAVs *in vivo* through proteolytic cleavage of their HA proteins. Hence, TMPRSS2 is a good target for the development of anti-IAV drugs. Such drugs could also be effective for many other respiratory viruses, including the recently emerged Middle East respiratory syndrome (MERS) coronavirus, because they are also activated by TMPRSS2 *in vitro*. Consequently, the present paper could have a large impact on the battle against respiratory virus infections and contribute greatly to human health.

Influenza A virus (IAV) is classified in the *Orthomyxoviridae* family and is a leading agent that affects and kills humans worldwide. IAV enters target cells via endocytosis, and virus-cell membrane fusion occurs at the late endosomes, thus releasing the viral genome to start virus replication. Membrane fusion is mediated by the hemagglutinin (HA) protein, which is synthesized as the inactive precursor HA_0 and cleaved by a host cell protease(s) to gain fusion activity. Proteolytic cleavage of HA_0 into the HA_1 and HA_2 subunits is essential for HA to express membrane fusion activity and, consequently, for IAV to acquire infectivity.

The HA of low-pathogenic (LP) IAVs, for which infection remains localized at respiratory and/or alimentary epithelial cells in birds and mammals, including humans, possesses a single arginine residue at the cleavage site. The HA of LP IAVs is thought to be cleaved and activated by a specific protease(s) present exclusively in these tissues. Trypsin, miniplasmin, tryptase Clara, mast cell tryptase, and type II transmembrane serine proteases (TTSPs) such as TMPRSS2, human airway trypsin-like protease (HAT), TMPRSS4, and matriptase have been shown to cleave the HA of LP IAVs at the single arginine residue (1, 2). Previous studies have also demonstrated HA subtype and strain specificities of TTSPs (3–6). On the other hand, the HA of high-pathogenic (HP) IAVs such as HP H5N1, which causes fatal systemic infections, contains multiple basic amino acids at the cleavage site (7–9). The HA of HP IAVs is cleaved by ubiquitous intracellular proteases such as furin and proprotein convertase 5/6, which are present in all cell types (1, 2). The concept of host protease-dependent tissue tro-

Received 11 December 2013 Accepted 27 February 2014
Published ahead of print 5 March 2014
Editor: T. S. Dermody
Address correspondence to Makoto Takeda, mtakeda@nih.go.jp.
Copyright © 2014, American Society for Microbiology. All Rights Reserved.
doi:10.1128/JVI.03677-13

Downloaded from http://jvi.asm.org/ on May 4, 2014 by Kyosuke Nagata

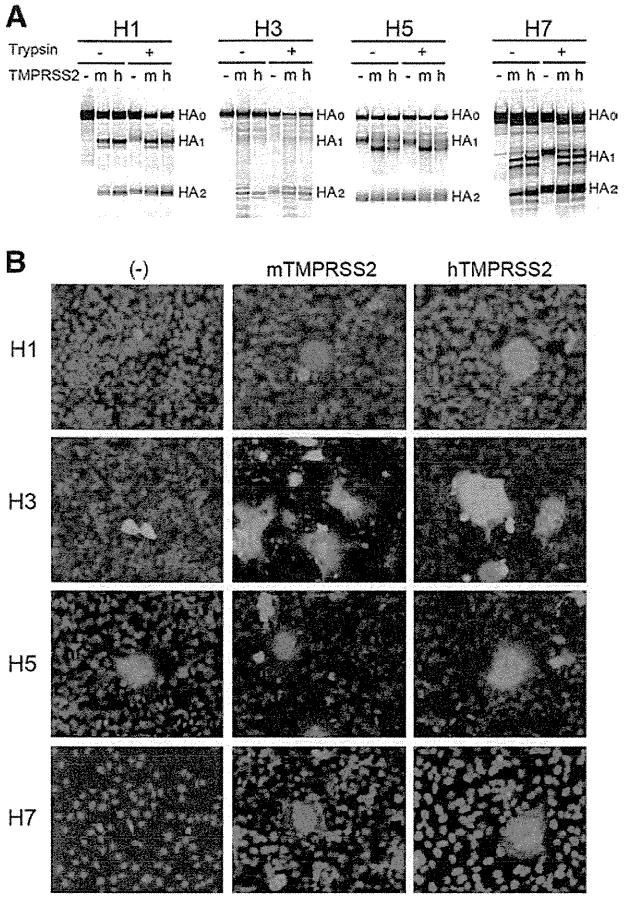

FIG 1 Proteolytic activation of HA by TMPRSS2. (A) HA proteins (H1, H3, H5, and H7 subtypes) were expressed alone (−) or together with mTMPRSS2 (m) or hTMPRSS2 (h) in 293T cells using expression plasmids. The cells were pulse labeled, and the HA components (HA_0, HA_1, and HA_2) were detected and analyzed by immunoprecipitation and SDS-PAGE. (B) HA proteins were expressed in HeLa/mTMPRSS2, HeLa/hTMPRSS2, or parental HeLa (−) cells. At 2 days posttransfection, the cells were treated with low-pH buffer (pH 5.3), and cell-cell fusion was analyzed by immunofluorescence staining using anti-IAV antibodies coupled with Alexa Fluor 488- or 549-conjugated secondary antibodies. The nuclear DNA was stained with DAPI.

pism and pathogenicity of LP and HP IAVs has been well established (7–9). However, the protease(s) directly involved in the cleavage activation of each HA subtype remains to be identified.

In the present study, we focused primarily on TMPRSS2 because this protease is expressed in the respiratory tract, activates a variety of respiratory viruses, and cleaves the HA of IAVs efficiently, even at marginal levels of expression, *in vitro* (4, 10–16). Our working hypothesis was that if TMPRSS2 is essential for IAV activation *in vivo*, mice lacking TMPRSS2 expression (TMPRSS2 knockout [KO] mice) are highly tolerant of challenge infection by IAVs that use primarily TMPRSS2 for HA cleavage.

MATERIALS AND METHODS

Ethics statement. All experiments with animals were performed in strict accordance with the animal experimentation guidelines of the National Institute of Infectious Diseases. The protocol was approved by the Institutional Animal Care and Use Committee of the institute (permit numbers 113066-II, 313008-II, and 13-09).

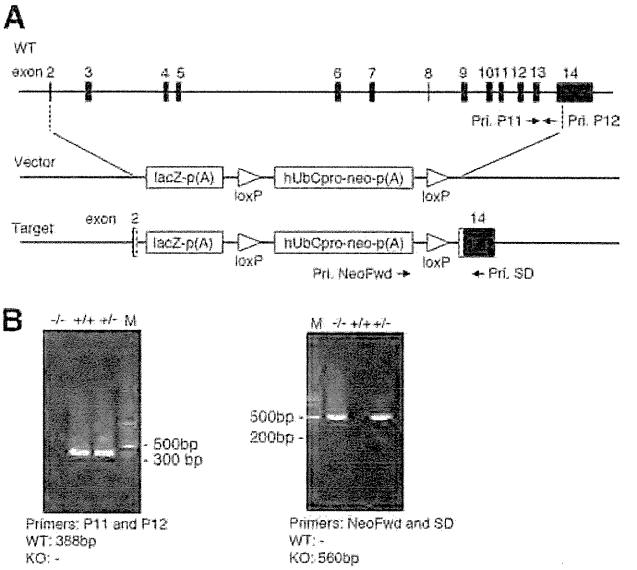

FIG 2 Structure of the targeted TMPRSS2 gene. (A) TMPRSS2 KO mice possess an allele [$Tmprss2^{tm1(KOMP)Vlcg}$] with an ablating deletion of the TMPRSS2 gene, which was replaced by the *lacZ* gene (VelociGene KOMP definitive null allele design). (B) The genotype was analyzed by VelociGene KOMP allele PCR genotyping strategies using primers NeoFwd and SD and a previously reported method using primers P11 and P12 (25).

TABLE 1 Transcriptome analysis of lungs from WT and TMPRSS2 KO mice for TTSPs

	RPKM			
	Lungs		Bronchi	
Gene	WT	KO	WT	KO
TTSPs				
Tmprss2	2.43	0.59[a]	3.62	0.51[a]
Tmprss3	0.00	0.00	0.21	0.00
Tmprss4	0.54	0.64	0.61	0.40
Tmprss5	0.05	0.21	1.61	0.38
Tmprss6	0.01	0.00	0.02	0.05
Tmprss7	0.39	0.00	0.01	0.03
Tmprss9	0.00	0.00	0.03	0.02
Tmprss11a	0.17	0.00	0.42	0.13
Tmprss11bnl	0.32	0.00	0.00	0.00
Tmprss11c	0.09	0.32	0.00	0.00
Tmprss11d	0.53	0.00	0.00	0.00
Tmprss11e	0.07	0.00	0.00	0.00
Tmprss11f	0.03	0.00	0.00	0.00
Tmprss11g	0.01	0.02	0.00	0.00
Tmprss12	0.00	0.00	0.00	0.00
Tmprss13	0.03	0.00	2.22	1.46
Tmprss15	0.01	0.02	0.11	0.07
Hpn	0.00	0.00	2.23	3.11
Lrp4	9.43	15.75	1.77	2.23
St14	0.35	4.35	12.96	13.74
Internal controls				
Gapdh	31.06	86.26	441.28	794.44
Actb	264.31	491.48	308.25	296.38

[a] Detected reads were mapped to exon 14 in the Tmprss2 coding sequence remaining in the TMPRSS2 KO mouse genome.

Downloaded from http://jvi.asm.org/ on May 4, 2014 by Kyosuke Nagata

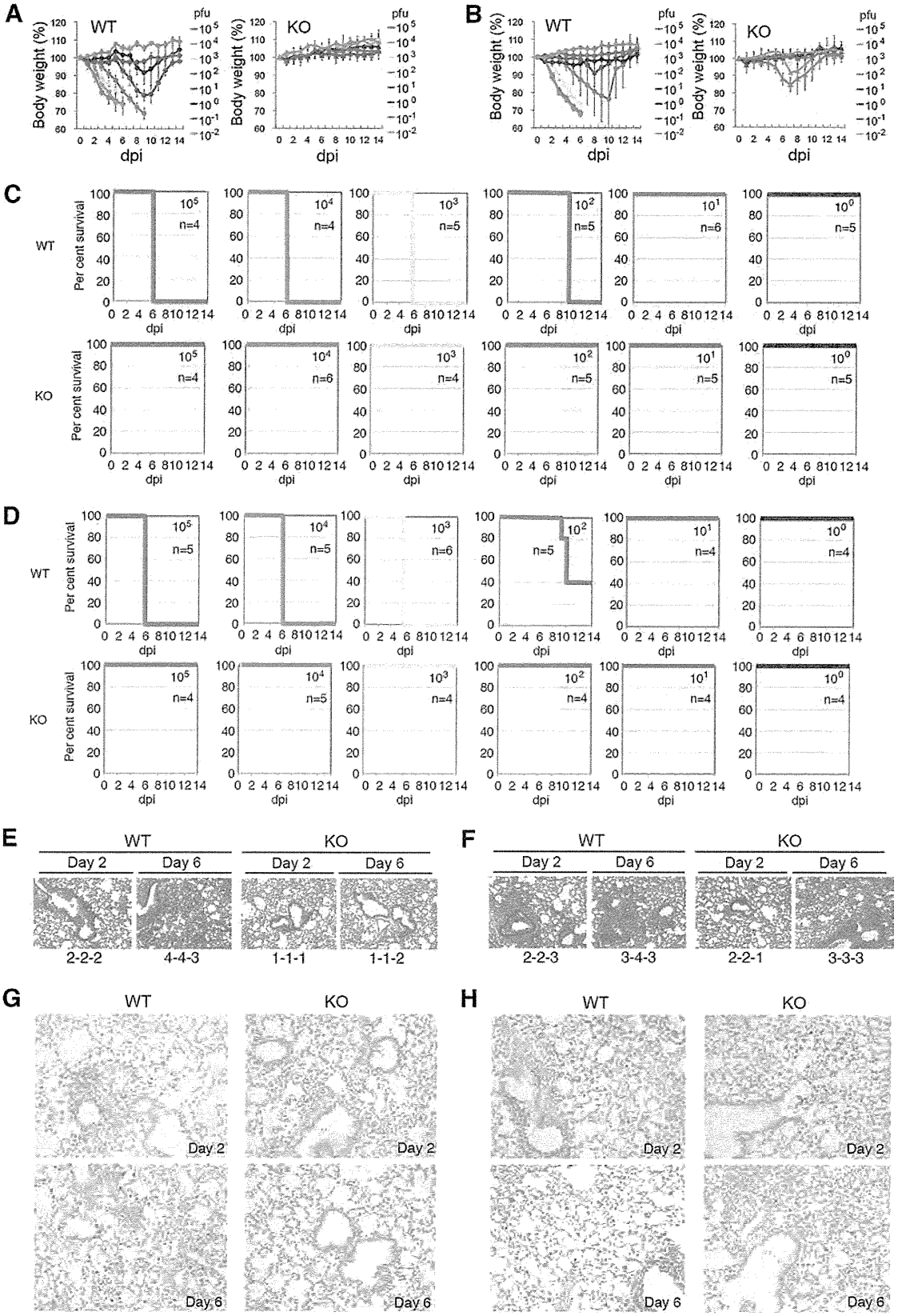

Downloaded from http://jvi.asm.org/ on May 4, 2014 by Kyosuke Nagata

Plasmids. A mouse TMPRSS2 (mTMPRSS2) expression plasmid, pTarget-mTMPRSS2, was generated by inserting the mTMPRSS2 cDNA obtained from a C57BL/6 mouse. The human TMPRSS2 (hTMPRSS2) expression plasmid pcDNA-TMPRSS2 was reported previously (11). IAV HA expression plasmids pCAGGS-H1, -H3, -H5, and -H7 were generated by inserting cDNAs of the HA-coding region from mouse-adapted (MA) A/California/04/09 (MA-CA04[H1N1]) (17), MA-A/Guizhou-X (MA-GZX[H3N2]) (18), A/Vietnam/1194/04 (VN1194[H5N1]) (19), and A/Anhui/1/2013 (Anhui1[H7N9]) (20), respectively.

Cells and viruses. MDCK, HeLa, and 293T cells were cultured in Dulbecco's modified Eagle's medium (DMEM) supplemented with 5% fetal calf serum (FCS). HeLa cells were transfected with pTarget-mTMPRSS2 or pcDNA-TMPRSS2, and Geneticin-resistant stable clones (HeLa/mTMPRSS2 and HeLa/hTMPRSS2, respectively) were selected in the presence of 1.0 mg/ml of Geneticin (G418; Nacalai Tesque). MA-CA04[H1N1] was generated by reverse genetics as reported previously (17). MA-GZX[H3N2], VN1194[H5N1], and Anhui1[H7N9] were reported previously (18–20).

Structural modeling of hTMPRSS2 and mTMPRSS2. No known structures of mTMPRSS2 or hTMPRSS2 are available. Therefore, three-dimensional structural models of hTMPRSS2 and mTMPRSS2 were generated by a homology modeling method using several protease structures as the templates. The I-TASSER modeling server (21) was used for modeling. The X-ray structure most similar to both TMPRSS2 models was the human transmembrane serine protease hepsin (PDB accession number 1Z8G). The models were refined by energy minimization using Swiss-PdbViewer (22) and finally evaluated by PROCHECK (23) and Verify3D (24).

Cell fusion assay. HeLa/mTMPRSS2, HeLa/hTMPRSS2, and parental HeLa cells were transfected with an HA-expressing plasmid (pCAGGS-H1, -H3, -H5, or -H7) by using X-tremeGENE HP DNA transfection reagent (Roche). At 2 days posttransfection, the cells were washed with phosphate-buffered saline (PBS) and treated with prewarmed low-pH buffer (145 mM NaCl, 20 mM sodium citrate [pH 5.3]) for 2 min. The low-pH buffer was then replaced with DMEM–5% FCS, and the cells were incubated at 37°C for 3 h. Cell-cell fusion was analyzed by immunofluorescence staining using anti-IAV rabbit serum against H7, anti-IAV goat serum against H3, and HA-specific rabbit monoclonal antibodies (clone 327 for H1 and clone 89 for H5) coupled with Alexa Fluor 488- or 549-conjugated secondary antibodies. The nuclear DNA was stained with 4′,6′-diamidino-2-phenylindole (DAPI).

Pulse labeling and immunoprecipitation. Monolayers of 293T cells were transfected with an HA-expressing plasmid (pCAGGS-H1, -H3, -H5, or -H7) alone or together with a TMPRSS2-expressing plasmid (pTarget-mTMPRSS2 or pcDNA-TMPRSS2). At 20 h posttransfection, the cells were cultured in methionine-cysteine-deficient medium for 1 h and then pulse labeled with [^{35}S]methionine-cysteine by using EasyTag EXPRE35S35S protein labeling mix (PerkinElmer) for 1 h. The cells in some wells were treated with 1 μg/ml acetylated trypsin (Sigma) for 1 h, as a trypsin-activated HA control, and all cells were lysed in radioimmunoprecipitation assay (RIPA) buffer. Polypeptides in the cell lysates were immunoprecipitated with anti-IAV rabbit sera against H3 and H7 (Sino Biological Inc.) and HA-specific rabbit monoclonal antibodies (clone 327 for H1 and clone 89 for H5) and analyzed by SDS-PAGE.

Generation of TMPRSS2 KO mice. TMPRSS2 gene KO C57BL/6 embryonic stem (ES) cells (product number VG13341) were obtained from the Knockout Mouse Project (KOMP) Repository (UC Davis). The ES cells possessed an allele [Tmprss2$^{tm1(KOMP)Vlcg}$] with an ablating deletion of the TMPRSS2 gene, which was replaced by the *lacZ* gene (VelociGene KOMP definitive null allele design). The ES cells were injected into C57BL/6 mouse blastocysts, and chimeric mice in a complete C57BL/6 genetic background were generated. Male chimeric mice were selected by VelociGene KOMP allele PCR genotyping strategies by using primers NeoFwd and SD and a previously reported method using primers P11 and P12 (25) and mated with normal female C57BL/6 mice to generate C57BL/6 mice with a heterozygous genotype of the TMPRSS2 gene (TMPRSS2$^{+/-}$). TMPRSS2 KO mice with a homologous genotype (TMPRSS2$^{-/-}$) were obtained by crossing male and female TMPRSS2$^{+/-}$ C57BL/6 mice.

Transcriptome analysis. The bronchi and right middle lobes of the lung were obtained from uninfected healthy wild-type (WT) and KO (TMPRSS2$^{-/-}$) mice (6-week-old females). Total RNA was prepared from ~50 mg of the bronchi or right middle lobes treated with RNAlater (Life Technologies), using a RecoverAll Total Nucleic Acid Isolation kit (Ambion), followed by selection of poly(A) mRNA using a FastTrack

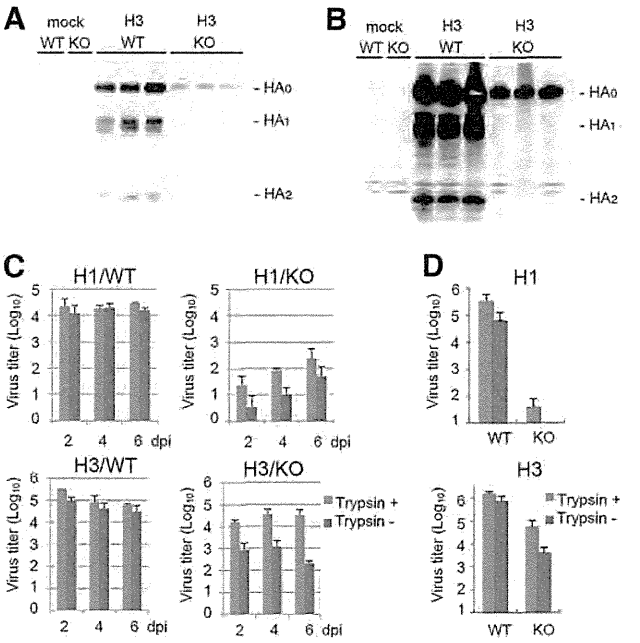

FIG 4 Proteolytic activation of IAVs *in vivo*. (A and B) WT and TMPRSS2 KO mice were intranasally inoculated with PBS (mock) (n = 1) or MA-GZX[H3N2] (n = 3). Lung lavage fluids (A) and lung homogenates (B) were collected at 6 dpi, and HA was analyzed by SDS-PAGE and immunoblotting. Each lane corresponds to data from an individual mouse. (C and D) WT and TMPRSS2 KO mice were intranasally inoculated with MA-CA04[H1N1] (n = 3) or MA-GZX[H3N2] (n = 3). Lung lavage fluids at 2, 4, and 6 dpi (C) and lung homogenates at 2 dpi (D) were either untreated (Trypsin −) or treated with trypsin (Trypsin +) and used for virus titration. Error bars represent standard deviations.

FIG 3 Role of TMPRSS2 in H1N1 and H3N2 IAV pathogenicity. (A and B) WT and TMPRSS2 KO mice were intranasally inoculated with different doses of MA-CA04[H1N1] (A) or MA-GZX[H3N2] (B) (n = 4 to 7). Body weights were measured daily. Error bars represent standard deviations. (C and D) Survival curves of IAV-infected mice. WT and TMPRSS2 KO mice were challenged with different doses of MA-CA04[H1N1] (C) or MA-GZX[H3N2] (D). For each experimental group, 4 to 6 mice were used. (E to H) Histopathological findings in the lungs of WT and TMPRSS2 KO mice infected with MA-CA04[H1N1] (E and G) or MA-GZX[H3N2] (F and H). Data obtained by hematoxylin and eosin staining (magnification, ×10) (E and F) and immunohistochemistry for the IAV nucleocapsid protein (magnification, ×10) (G and H) are shown. The inflammation scores of individual mice (n = 3) are shown at the bottom of each panel (E and F): 0, no apparent changes; 1, minimal changes or bronchiolitis; 2, bronchiolitis and/or slight alveolitis; 3, mild alveolitis with neutrophils, monocytes/macrophages, or lymphocytes; 4, moderate alveolitis.

Downloaded from http://jvi.asm.org/ on May 4, 2014 by Kyosuke Nagata

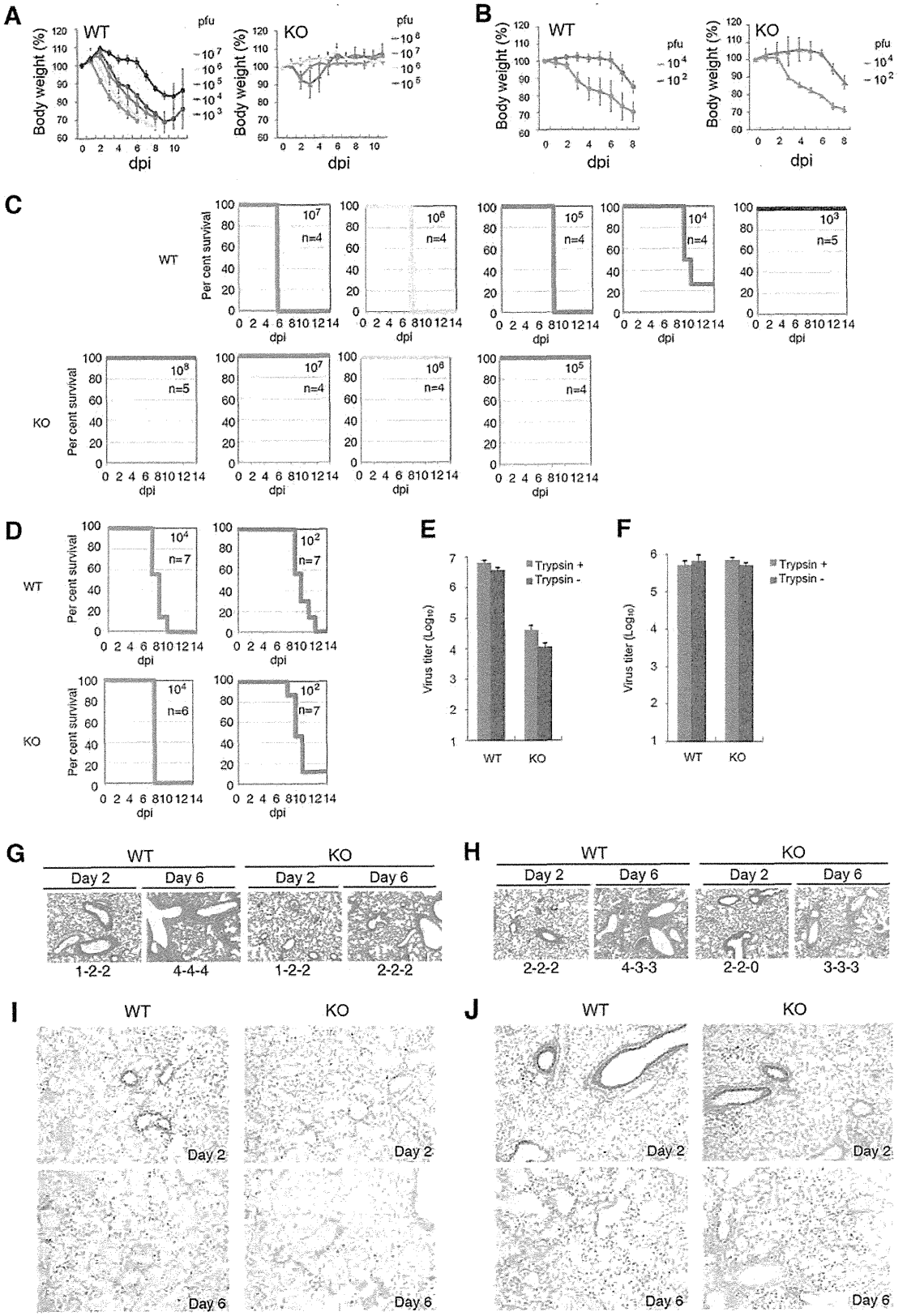

Downloaded from http://jvi.asm.org/ on May 4, 2014 by Kyosuke Nagata

MAG mRNA isolation kit (Invitrogen). RNA strand-specific transcriptome sequencing (RNA-seq) libraries were prepared from ~50 ng of the purified poly(A) mRNA using a ScriptSeq v2 RNA-Seq Library Preparation kit (Epicentre). The prepared RNA-seq library was sequenced by using a GAIIx sequencer (Illumina). The obtained strand-specific short reads were analyzed by CLC Genome Workbench (v. 6.05) with mean expression normalization against *Mus musculus* reference genome sequences (GRCm38.p1), and genes showing significant differential expression were detected with a false discovery rate (FDR) of <0.05 and changes of $\geq$2-fold. The reads per kilobase of exon model per million mapped reads (RPKM) were estimated for each transcriptome experiment.

Titration of infectious units. To determine the infectious virus titers activated *in vivo*, monolayers of MDCK cells in 12-well plates were infected with serially diluted virus samples for 1 h at 4°C, washed twice with PBS, overlaid with DMEM–1% agarose, and incubated for 24 h at 37°C to allow the viruses to enter the cells. Trypsin was omitted to avoid HA cleavage before virus entry. At 24 h postinfection, the cell monolayers were additionally overlaid with DMEM–1% agarose supplemented with 2.0 μg/ml of trypsin to allow plaque formation. The virus titers obtained with this method were essentially equivalent to those obtained by immunofluorescence staining techniques (26), in which trypsin was omitted during the entire process of titration and individual infected cells, instead of plaques, were detected and counted. To determine the infectious titers of viruses that had not been activated *in vivo* but possessed infectious potential, virus samples were treated with 1.0 μg/ml of trypsin and subjected to a standard plaque assay.

Infection of mice. KO (TMPRSS2$^{-/-}$) and WT (TMPRSS2$^{+/+}$) C57BL/6 mice (6- to 7-week-old males or females) were challenged with MA-CA04[H1N1], MA-GZX[H3N2], VN1194[H5N1], or Anhui1 [H7N9]. For each mouse, 20 μl of virus solution containing different amounts of IAV was inoculated intranasally. For mock infection, the same volume of PBS was used. For each experimental group, 4 to 6 mice were used to monitor body weight. To analyze the *in vivo* activation and replication of IAV, WT and TMPRSS2 KO mice were challenged with 4.0×10^3 PFU of MA-CA04[H1N1] or 6.8×10^3 PFU of MA-GZX[H3N2]. Lung lavage fluids collected at 2, 4, and 6 days postinfection (dpi) and lung homogenates collected at 2 dpi were either untreated or treated with trypsin to determine the virus titers activated *in vivo* and *in vitro*, respectively. Three mice were used for each experimental group, and samples were collected separately from individual mice. For histopathological examinations, WT and TMPRSS2 KO mice were infected with 4.0×10^3 PFU (3.0×10^2 50% lethal doses [LD_{50}]) of MA-CA04[H1N1], 6.8×10^3 PFU (1.0×10^2 LD_{50}) of MA-GZX[H3N2], 1.0×10^4 PFU (1.0×10^2 LD_{50}) of VN1194[H5N1], or 4.0×10^6 PFU (1.0×10^2 LD_{50}) of Anhui1[H7N9]; euthanized; and autopsied at 2 and 6 dpi. Three mice were used for each experimental group.

Immunoblotting. The lung lavage fluids and lung homogenates were mixed with lysis buffer to make a final solution containing 150 mM NaCl, 50 mM Tris-HCl (pH 7.5), 4 mM EDTA, 0.1% sodium deoxycholate, 1% Nonidet P-40, and 0.1% SDS, containing a complete protease inhibitor mixture (Roche Diagnostics). The polypeptides were then separated by SDS-PAGE and immunoblotted. A rabbit antiserum raised against H3 (Sino Biological Inc.) was used for detection.

Nucleotide sequence accession number. The RNA-seq reads of the lung tissues from WT and TMPRSS2 KO mice are available at the DDBJ Sequence Read Archive under accession number DRA001103 (47,935,571 and 46,863,938 paired-end reads for WT and TMPRSS2 KO mice, respectively).

RESULTS

mTMPRSS2 proteolytically activates IAV HAs similarly to hTMPRSS2. To obtain a biological rationale for performing mouse experiments, we analyzed mTMPRSS2. Three-dimensional structural models of mTMPRSS2 and hTMPRSS2 showed strong conservation of amino acid residues near the protease active site (data not shown). Based on the strong homology between hTMPRSS2 and mTMPRSS2, these proteases were strongly suggested to have similar substrate specificities. However, the TMPRSS2 structures were strictly models, and biological analyses were performed. The analyses showed that all HAs of LP IAVs of the H1, H3, and H7 subtypes were cleaved by both mTMPRSS2 and hTMPRSS2 (Fig. 1A), and the cleaved HAs showed cell-cell fusion (syncytium formation) activity (Fig. 1B). As expected, cleavage and activation of HA of an HP IAV of the H5 subtype occurred independently of TMPRSS2 expression (Fig. 1A and B). Consistent with previous data (27), different molecular sizes of HA were detected in TMPRSS2-expressing cells, because the expression of TMPRSS2 modulates the HA glycosylation pattern (Fig. 1A).

TMPRSS2 is essential for the pathogenicity of H1N1 and H3N2 IAVs. TMPRSS2 KO mice, which possessed an ablating deletion including exons 3 to 13 of the TMPRSS2 gene, were generated in a complete C57BL/6 genetic background (Fig. 2). To confirm whether TMPRSS2 KO induced unexpected differential expression of other TTSPs, RNA-seq experiments were performed. The transcriptome analysis indicated that TMPRSS2 KO did not significantly affect the expressions of other TTSP genes and potential protease genes (Table 1). As an exception, the level of St14 appeared to be increased in the TMPRSS2 KO mouse lung (Table 1), but the raw count was still very low, and the change was judged to be insignificant based on the FDR analysis. However, our data did not exclude the possibility that the change was induced by TMPRSS2 gene KO. TMPRSS2 KO mice exhibited normal reproduction, development, and growth patterns, similarly to WT C57BL/6 mice, as observed for previously reported TMPRSS2 KO mice with a deletion of exons 10 to 13 in the TMPRSS2 gene (25).

Various doses of MA viruses of human LP IAV strains MA-CA04[H1N1] and MA-GZX[H3N2] were inoculated intranasally into WT and TMPRSS2 KO mice. All WT mice inoculated with $\geq 10^2$ PFU (7.5 LD_{50}) of MA-CA04[H1N1] died or required euthanasia (Fig. 3A and C). In strong contrast, TMPRSS2 KO mice challenged with up to 10^5 PFU (7.5×10^3 LD_{50}) showed neither clinical signs nor body weight loss (Fig. 3A and C). TMPRSS2 KO mice were also highly tolerant of lethal challenge infections with MA-

FIG 5 Role of TMPRSS2 in H5N1 and H7N9 IAV pathogenicity. (A and B) WT and TMPRSS2 KO mice were intranasally inoculated with different doses of Anhui1[H7N9] (A) or VN1194[H5N1] (B) ($n = 4$ to 6). The body weights were measured daily. Error bars represent standard deviations. (C and D) Survival curves of IAV-infected mice. WT and TMPRSS2 KO mice were challenged with different doses of Anhui1[H7N9] (C) or VN1194[H5N1] (D). For each experimental group, 4 to 7 mice were used. (E and F) WT and TMPRSS2 KO mice were intranasally inoculated with Anhui1[H7N9] ($n = 3$) or VN1194[H5N1] ($n = 3$). Lung homogenates at 4 dpi (D) were either untreated (Trypsin −) or treated with trypsin (Trypsin +) and used for virus titration. Error bars represent standard deviations. (G to J) Histopathological findings in the lungs of WT and TMPRSS2 KO mice infected with Anhui1[H7N9] (G and I) or VN1194[H5N1] (H and J). Data obtained by hematoxylin and eosin staining (magnification, ×10) (G and H) and immunohistochemistry for the IAV nucleocapsid protein (magnification, ×10) (I and J) are shown. The inflammation scores of individual mice ($n = 3$) are shown at the bottom of each panel (G and H): 0, no apparent changes; 1, minimal changes or bronchiolitis; 2, bronchiolitis and/or slight alveolitis; 3, mild alveolitis with neutrophils, monocytes/macrophages, or lymphocytes; 4, moderate alveolitis.

Downloaded from http://jvi.asm.org/ on May 4, 2014 by Kyosuke Nagata

GZX[H3N2] (Fig. 3B and D). All TMPRSS2 KO mice infected with 10^5 PFU (1.5×10^3 LD_{50}) of MA-GZX[H3N2] showed moderate body weight loss but recovered completely (Fig. 3B and D).

Figure 3E to H shows the histopathology of lungs of mice infected with 4.0×10^3 PFU (3.0×10^2 LD_{50}) of MA-CA04[H1N1] or 6.8×10^3 PFU (1.0×10^2 LD_{50}) of MA-GZX[H3N2]. WT mice infected with each virus developed bronchiolitis and peribronchial inflammation, with a few foci of alveolitis at 2 dpi and mild to moderate alveolitis at 6 dpi (Fig. 3E and F). Viral antigens were detected in bronchial epithelial cells and alveolar lining cells in the lungs of WT mice at 2 dpi and had spread dramatically to the entire lungs by 6 dpi (Fig. 3G and H). In contrast, the lungs of KO mice infected with the same viruses exhibited significantly reduced levels of inflammation (Fig. 3E and F). Viral antigen-positive cells did not spread during the observation period (Fig. 3G and H). Viral antigens were almost completely eliminated from bronchiolar epithelial cells of KO mice by 6 dpi (Fig. 3G and H).

TMPRSS2 is essential for proteolytic activation of IAVs *in vivo*. To explore the cleavage of HA in the lungs, WT and TMPRSS2 KO mice were infected with 4.0×10^3 PFU (3.0×10^2 LD_{50}) of MA-CA04[H1N1] or 6.8×10^3 PFU (1.0×10^2 LD_{50}) of MA-GZX[H3N2]. At 6 dpi, lung lavage fluids were collected from mice infected with MA-GZX[H3N2] and analyzed for HA protein by SDS-PAGE and immunoblotting. Cleavage of HA was demonstrated in WT mice, as signals for the HA_1 and HA_2 subunits were clearly detected in these mice (Fig. 4A). In contrast, only the HA_0 precursor was detected in TMPRSS2 KO mice, and HA_1 and HA_2 remained undetectable (Fig. 4A). Similarly, lung homogenates of the infected mice were analyzed. HA was efficiently cleaved into HA_1 and HA_2 in the lung homogenates of WT mice (Fig. 4B). Meanwhile, the lung homogenates of TMPRSS2 KO mice showed HA_0 signals, but HA_1 and HA_2 were undetectable (Fig. 4B). These findings indicated that the HA protein of progeny viruses present in the respiratory tract had been cleaved in WT mice, while HA cleavage was severely impaired in TMPRSS2 KO mice. To verify whether the infectivity of the progeny viruses from each mouse lung was activated *in vivo*, lung lavage fluids at 2, 4, and 6 dpi and lung homogenates at 2 dpi were treated or untreated with trypsin *in vitro* and compared for infectivity *in vitro* to determine virus titers. At 2 dpi, the virus titers of MA-CA04[H1N1] and MA-GZX[H3N2] reached their peak levels in WT mice (Fig. 4C). The HAs of progeny viruses were shown to be fully activated in WT mice, since the virus infectivity titers without trypsin treatment (Fig. 4C and D) were similar to those after activation *in vitro* (Fig. 4C and D). The virus titers in the lungs of TMPRSS2 KO mice were much lower than those in the lungs of WT mice (Fig. 4C and D), showing restricted virus growth in TMPRSS2 KO mice. Importantly, the virus titers (Fig. 4C and D) were further increased 10 to 100 times after trypsin treatment *in vitro* (Fig. 4C and D). These data demonstrated that the great majority (90 to 99%) of the progeny virus particles failed to be proteolytically activated in TMPRSS2 KO mice.

TMPRSS2 is essential for LP H7N9 IAV, but dispensable for HP H5N1 IAV, to exhibit pathogenicity. The pathogenicity of a human isolate of an emerging LP H7N9 subtype virus, Anhui1 [H7N9], was also analyzed. Anhui1[H7N9] was inoculated intranasally into WT and TMPRSS2 KO mice. As shown in Fig. 5A and C, TMPRSS2 KO mice were highly tolerant of H7N9 virus infection. All WT mice infected with 10^5 PFU (5.0×10 LD_{50}) of Anhui1[H7N9] died or required euthanasia by 8 dpi (Fig. 5A and C). In contrast, all TMPRSS2 KO mice infected with the same dose (10^5 PFU [5.0×10 LD_{50}]) showed no clinical signs, and those infected with a 1,000-times-higher dose, 10^8 PFU (5.0×10^4 LD_{50}), showed only temporary and mild body weight loss (Fig. 5A). The virus titers in the KO mouse lungs were much lower than those in the WT mouse lungs (Fig. 5E). Histopathological examinations of mouse lungs infected with 4.0×10^6 PFU of Anhui1[H7N9] showed that Anhui1[H7N9] spread poorly in the lungs of TMPRSS2 KO mice (Fig. 5G and I).

In contrast to the findings for the LP IAVs described above, a human isolate of an HP H5N1 subtype virus, VN1194[H5N1], caused severe body weight loss, neurological symptoms, and death or requirement for euthanasia by 8 or 9 dpi in both WT and TMPRSS2 KO mice infected with 10^4 PFU (2.0×10^3 LD_{50}) of VN1194[H5N1] (Fig. 5B and D). The survival curves of WT and TMPRSS2 KO mice infected with 10^2 PFU (5.0×10 LD_{50}) of VN1194[H5N1] were also similar to one another (Fig. 5B and D). The virus titers in the lungs were equivalent between WT and KO mice (Fig. 5F). Histopathological examinations of mouse lungs infected with 1.0×10^4 PFU of VN1194[H5N1] demonstrated that VN1194[H5N1] spread efficiently in a similar manner in the lungs of WT and TMPRSS2 KO mice (Fig. 5H and J). The overall results indicated that, unlike LP IAVs, proteolytic activation of the HP H5N1 virus occurred in mouse lungs independently of TMPRSS2.

DISCUSSION

In the last decade, we have experienced outbreaks of a swine-origin LP H1N1 IAV and the severe acute respiratory syndrome (SARS) coronavirus (28, 29). These outbreaks proved that respiratory viruses can currently spread rapidly and that the available strategies are insufficiently effective to prevent global transmission of emerging respiratory viruses (28). At this time, H5N1 and H7N9 IAVs and the Middle East respiratory syndrome (MERS) coronavirus are potential threats for humans (29, 30).

The present study has provided concrete evidence that TMPRSS2 expression is essential for *in vivo* replication of emerging H7N9 and seasonal IAVs and that this protease primarily determines IAV pathogenicity. Based on the strong homology between hTMPRSS2 and mTMPRSS2, hTMPRSS2 is strongly suggested to play a similar role in the activation and pathogenicity of human IAVs *in vivo*. In human airway bronchial epithelial cells, TMPRSS2 is expressed by type 1 and type 2 pneumocytes of the alveolar epithelium and alveolar macrophages (12, 31). In the airway, IAV particles are released exclusively from the apical membrane (32). To achieve this, the IAV HA protein is specifically targeted to the apical plasma membrane (33, 34), and TMPRSS2 is selectively expressed at the apical membrane of airway epithelial cells (35). Taking these data into consideration, it is most likely that LP IAVs use primarily the specific host protease TMPRSS2 for HA activation in the lungs. However, our data do not exclude the possibility that TMPRSS2 may activate a precursor of another protease(s) that finally induces HA activation. Nevertheless, our data showing the critical role of TMPRSS2 expressed in the respiratory tract in the activation of IAV pathogenicity *in vivo* support the concept of host protease-mediated pathogenicity of IAVs (7–9).

The present findings suggest that TMPRSS2 is a good target for the development of anti-LP IAV drugs. The membrane-anchoring and cytoplasmic domains of TTSPs regulate cellular trafficking

Downloaded from http://jvi.asm.org/ on May 4, 2014 by Kyosuke Nagata

and localization of TTSPs, thereby enabling temporal and spatial regulation of substrate processing (36–38). Accordingly, by targeting specific substrates such as peptide hormones, growth factors, differentiation factors, receptors, and adhesion molecules, TTSPs play a variety of critical roles in developmental stages and physiological events (36–38). A previous study suggested that TMPRSS2 regulates Na^+ currents (39). However, the physiological roles of TMPRSS2 remain to be elucidated (40), because TMPRSS2 KO mice showed a normal phenotype.

During the submission process for the present paper, Hatesuer et al. (41) reported a similar study demonstrating a critical role of TMPRSS2 in the pathogenicity of H1N1 and H3N2 IAVs in mice. They used a previously reported TMPRSS2 KO mouse strain with a deletion of exons 10 to 13 in the TMPRSS2 gene (25, 41). The TMPRSS2 KO mice with a deletion of exons 3 to 13 in the TMPRSS2 gene established in the present study exhibited phenotypes very similar to those of their mice, providing a very strong conclusion that TMPRSS2 expression is essential for IAV pathogenesis. Interestingly, in agreement with their data (41), our study demonstrated that replication of H1N1 IAV was more severely restricted in TMPRSS2 KO mice than that of H3N2 IAV. Therefore, cleavage of the H1 subtype appears to be more strongly dependent on TMPRSS2 expression than cleavage of the H3 subtype.

Finally, TTSPs have a clear substrate specificity (37). Nevertheless, various respiratory viruses, including the SARS coronavirus (12, 42–44), MERS coronavirus (14), human metapneumovirus (11), and parainfluenza viruses (13), also use TMPRSS2 for their activation. These observations imply that a variety of respiratory viruses may specifically exploit TMPRSS2 for activation. Drugs that inhibit TMPRSS2 are therefore expected to be effective against a wide spectrum of respiratory viruses. Meanwhile, different types of drugs targeting ubiquitous proteases other than TMPRSS2 may be required for HP IAVs such as the H5N1 virus subtype.

ACKNOWLEDGMENTS

The ES cells used for this research project were generated by the Trans-NIH Knockout Mouse Project (KOMP) and obtained from the KOMP Repository (http://www.komp.org/). NIH grants to VelociGene at Regeneron Inc. (U01HG004085) and the CSD Consortium (U01HG004080) funded the generation of gene-targeted ES cells for 8,500 genes in the KOMP Program, which were archived and distributed by the KOMP Repository at UC Davis and CHORI (U42RR024244). This work was supported by grants-in-aid from the Ministry of Education, Science, Sports and Culture of Japan (KAKENHI; 23390114), the Takeda Science Foundation, and ERATO, Japan, and by a National Institute of Allergy and Infectious Diseases Public Health Service research grant.

We thank Yuelong Shu, Chinese Center for Disease Control and Prevention, and Le Quynh Mai, National Institute of Hygiene and Epidemiology, for providing H7N9 IAV and H5N1 IAV, respectively; R. A. Lamb, Northwestern University, for providing anti-IAV serum; and E. Takashita, M. Shirakura, H. Asanuma, H. Fukuhara, A. Sato, N. Nagata, Y. Sato, and all our members in the Department of Virology 3, NIID, for suggestions and technical support.

REFERENCES

1. Kido H, Okumura Y, Takahashi E, Pan HY, Wang S, Yao D, Yao M, Chida J, Yano M. 2012. Role of host cellular proteases in the pathogenesis of influenza and influenza-induced multiple organ failure. Biochim. Biophys. Acta 1824:186–194. http://dx.doi.org/10.1016/j.bbapap.2011.07.001.
2. Bottcher-Friebertshauser E, Klenk HD, Garten W. 2013. Activation of influenza viruses by proteases from host cells and bacteria in the human airway epithelium. Pathog. Dis. 69:87–100. http://dx.doi.org/10.1111/2049-632X.12053.
3. Beaulieu A, Gravel E, Cloutier A, Marois I, Colombo E, Desilets A, Verreault C, Leduc R, Marsault E, Richter MV. 2013. Matriptase proteolytically activates influenza virus and promotes multicycle replication in the human airway epithelium. J. Virol. 87:4237–4251. http://dx.doi.org/10.1128/JVI.03005-12.
4. Baron J, Tarnow C, Mayoli-Nussle D, Schilling E, Meyer D, Hammami M, Schwalm F, Steinmetzer T, Guan Y, Garten W, Klenk HD, Bottcher-Friebertshauser E. 2013. Matriptase, HAT, and TMPRSS2 activate the hemagglutinin of H9N2 influenza A viruses. J. Virol. 87:1811–1820. http://dx.doi.org/10.1128/JVI.02320-12.
5. Galloway SE, Reed ML, Russell CJ, Steinhauer DA. 2013. Influenza HA subtypes demonstrate divergent phenotypes for cleavage activation and pH of fusion: implications for host range and adaptation. PLoS Pathog. 9:e1003151. http://dx.doi.org/10.1371/journal.ppat.1003151.
6. Hamilton BS, Gludish DW, Whittaker GR. 2012. Cleavage activation of the human-adapted influenza virus subtypes by matriptase reveals both subtype and strain specificities. J. Virol. 86:10579–10586. http://dx.doi.org/10.1128/JVI.00306-12.
7. Bosch FX, Garten W, Klenk HD, Rott R. 1981. Proteolytic cleavage of influenza virus hemagglutinins: primary structure of the connecting peptide between HA1 and HA2 determines proteolytic cleavability and pathogenicity of avian influenza viruses. Virology 113:725–735. http://dx.doi.org/10.1016/0042-6822(81)90201-4.
8. Kawaoka Y, Webster RG. 1988. Sequence requirements for cleavage activation of influenza virus hemagglutinin expressed in mammalian cells. Proc. Natl. Acad. Sci. U. S. A. 85:324–328. http://dx.doi.org/10.1073/pnas.85.2.324.
9. Rott R, Klenk HD, Nagai Y, Tashiro M. 1995. Influenza viruses, cell enzymes, and pathogenicity. Am. J. Respir. Crit. Care Med. 152:S16–S19. http://dx.doi.org/10.1164/ajrccm/152.4_Pt_2.S16.
10. Bottcher E, Matrosovich T, Beyerle M, Klenk HD, Garten W, Matrosovich M. 2006. Proteolytic activation of influenza viruses by serine proteases TMPRSS2 and HAT from human airway epithelium. J. Virol. 80:9896–9898. http://dx.doi.org/10.1128/JVI.01118-06.
11. Shirogane Y, Takeda M, Iwasaki M, Ishiguro N, Takeuchi H, Nakatsu Y, Tahara M, Kikuta H, Yanagi Y. 2008. Efficient multiplication of human metapneumovirus in Vero cells expressing the transmembrane serine protease TMPRSS2. J. Virol. 82:8942–8946. http://dx.doi.org/10.1128/JVI.00676-08.
12. Matsuyama S, Nagata N, Shirato K, Kawase M, Takeda M, Taguchi F. 2010. Efficient activation of the severe acute respiratory syndrome coronavirus spike protein by the transmembrane protease TMPRSS2. J. Virol. 84:12658–12664. http://dx.doi.org/10.1128/JVI.01542-10.
13. Abe M, Tahara M, Sakai K, Yamaguchi H, Kanou K, Shirato K, Kawase M, Noda M, Kimura H, Matsuyama S, Fukuhara H, Mizuta K, Maenaka K, Ami Y, Esumi M, Kato A, Takeda M. 2013. TMPRSS2 is an activating protease for respiratory parainfluenza viruses. J. Virol. 87:11930–11935. http://dx.doi.org/10.1128/JVI.01490-13.
14. Shirato K, Kawase M, Matsuyama S. 2013. Middle East respiratory syndrome coronavirus (MERS-CoV) infection mediated by the transmembrane serine protease TMPRSS2. J. Virol. 87:12552–12561. http://dx.doi.org/10.1128/JVI.01890-13.
15. Gierer S, Bertram S, Kaup F, Wrensch F, Heurich A, Kramer-Kuhl A, Welsch K, Winkler M, Meyer B, Drosten C, Dittmer U, von Hahn T, Simmons G, Hofmann H, Pohlmann S. 2013. The spike protein of the emerging betacoronavirus EMC uses a novel coronavirus receptor for entry, can be activated by TMPRSS2, and is targeted by neutralizing antibodies. J. Virol. 87:5502–5511. http://dx.doi.org/10.1128/JVI.00128-13.
16. Bertram S, Dijkman R, Habjan M, Heurich A, Gierer S, Glowacka I, Welsch K, Winkler M, Schneider H, Hofmann-Winkler H, Thiel V, Pohlmann S. 2013. TMPRSS2 activates the human coronavirus 229E for cathepsin-independent host cell entry and is expressed in viral target cells in the respiratory epithelium. J. Virol. 87:6150–6160. http://dx.doi.org/10.1128/JVI.03372-12.
17. Sakabe S, Ozawa M, Takano R, Iwastuki-Horimoto K, Kawaoka Y. 2011. Mutations in PA, NP, and HA of a pandemic (H1N1) 2009 influenza virus contribute to its adaptation to mice. Virus Res. 158:124–129. http://dx.doi.org/10.1016/j.virusres.2011.03.022.
18. Yoshikawa T, Matsuo K, Matsuo K, Suzuki Y, Nomoto A, Tamura S, Kurata T, Sata T. 2004. Total viral genome copies and virus-Ig complexes

Downloaded from http://jvi.asm.org/ on May 4, 2014 by Kyosuke Nagata

after infection with influenza virus in the nasal secretions of immunized mice. J. Gen. Virol. 85:2339–2346. http://dx.doi.org/10.1099/vir.0.79892-0.
19. Gao P, Watanabe S, Ito T, Goto H, Wells K, McGregor M, Cooley AJ, Kawaoka Y. 1999. Biological heterogeneity, including systemic replication in mice, of H5N1 influenza A virus isolates from humans in Hong Kong. J. Virol. 73:3184–3189.
20. Watanabe T, Kiso M, Fukuyama S, Nakajima N, Imai M, Yamada S, Murakami S, Yamayoshi S, Iwatsuki-Horimoto K, Sakoda Y, Takashita E, McBride R, Noda T, Hatta M, Imai H, Zhao D, Kishida N, Shirakura M, de Vries RP, Shichinohe S, Okamatsu M, Tamura T, Tomita Y, Fujimoto N, Goto K, Katsura H, Kawakami E, Ishikawa I, Watanabe S, Ito M, Sakai-Tagawa Y, Sugita Y, Uraki R, Yamaji R, Eisfeld AJ, Zhong G, Fan S, Ping J, Maher EA, Hanson A, Uchida Y, Saito T, Ozawa M, Neumann G, Kida H, Odagiri T, Paulson JC, Hasegawa H, Tashiro M, Kawaoka Y. 2013. Characterization of H7N9 influenza A viruses isolated from humans. Nature 501:551–555. http://dx.doi.org/10.1038/nature12392.
21. Roy A, Kucukural A, Zhang Y. 2010. I-TASSER: a unified platform for automated protein structure and function prediction. Nat. Protoc. 5:725–738. http://dx.doi.org/10.1038/nprot.2010.5.
22. Guex N, Peitsch MC. 1997. SWISS-MODEL and the Swiss-PdbViewer: an environment for comparative protein modeling. Electrophoresis 18:2714–2723. http://dx.doi.org/10.1002/elps.1150181505.
23. Laskowski RA, MacArthur MW, Moss DS, Thornton MJ. 1993. PROCHECK: a program to check the stereochemistry of protein structures. J. Appl. Crystallogr. 26:283–291. http://dx.doi.org/10.1107/S0021889892009944.
24. Eisenberg D, Luthy R, Bowie JU. 1997. VERIFY3D: assessment of protein models with three-dimensional profiles. Methods Enzymol. 277:396–404. http://dx.doi.org/10.1016/S0076-6879(97)77022-8.
25. Kim TS, Heinlein C, Hackman RC, Nelson PS. 2006. Phenotypic analysis of mice lacking the Tmprss2-encoded protease. Mol. Cell. Biol. 26:965–975. http://dx.doi.org/10.1128/MCB.26.3.965-975.2006.
26. Tashiro M, Ciborowski P, Klenk HD, Pulverer G, Rott R. 1987. Role of Staphylococcus protease in the development of influenza pneumonia. Nature 325:536–537. http://dx.doi.org/10.1038/325536a0.
27. Bertram S, Glowacka I, Blazejewska P, Soilleux E, Allen P, Danisch S, Steffen I, Choi SY, Park Y, Schneider H, Schughart K, Pohlmann S. 2010. TMPRSS2 and TMPRSS4 facilitate trypsin-independent spread of influenza virus in Caco-2 cells. J. Virol. 84:10016–10025. http://dx.doi.org/10.1128/JVI.00239-10.
28. Waterer G. 2011. Controlling epidemic viral infection. Curr. Opin. Infect. Dis. 24:130–136. http://dx.doi.org/10.1097/QCO.0b013e328343b720.
29. Graham RL, Donaldson EF, Baric RS. 2013. A decade after SARS: strategies for controlling emerging coronaviruses. Nat. Rev. Microbiol. 11:836–848. http://dx.doi.org/10.1038/nrmicro3143.
30. Cowling BJ, Jin L, Lau EH, Liao Q, Wu P, Jiang H, Tsang TK, Zheng J, Fang VJ, Chang Z, Ni MY, Zhang Q, Ip DK, Yu J, Li Y, Wang L, Tu W, Meng L, Wu JT, Luo H, Li Q, Shu Y, Li Z, Feng Z, Yang W, Wang Y, Leung GM, Yu H. 2013. Comparative epidemiology of human infections with avian influenza A H7N9 and H5N1 viruses in China: a population-based study of laboratory-confirmed cases. Lancet 382:129–137. http://dx.doi.org/10.1016/S0140-6736(13)61171-X.
31. Bertram S, Heurich A, Lavender H, Gierer S, Danisch S, Perin P, Lucas JM, Nelson PS, Pohlmann S, Soilleux EJ. 2012. Influenza and SARS-coronavirus activating proteases TMPRSS2 and HAT are expressed at multiple sites in human respiratory and gastrointestinal tracts. PLoS One 7:e35876. http://dx.doi.org/10.1371/journal.pone.0035876.
32. Rodriguez Boulan E, Sabatini DD. 1978. Asymmetric budding of viruses in epithelial monlayers [*sic*]: a model system for study of epithelial polarity. Proc. Natl. Acad. Sci. U. S. A. 75:5071–5075. http://dx.doi.org/10.1073/pnas.75.10.5071.
33. Nayak DP, Barman S. 2002. Role of lipid rafts in virus assembly and budding. Adv. Virus Res. 58:1–28. http://dx.doi.org/10.1016/S0065-3527(02)58001-5.
34. Takeda M, Leser GP, Russell CJ, Lamb RA. 2003. Influenza virus hemagglutinin concentrates in lipid raft microdomains for efficient viral fusion. Proc. Natl. Acad. Sci. U. S. A. 100:14610–14617. http://dx.doi.org/10.1073/pnas.2235620100.
35. Jacquinet E, Rao NV, Rao GV, Hoidal JR. 2000. Cloning, genomic organization, chromosomal assignment and expression of a novel mosaic serine proteinase: epitheliasin. FEBS Lett. 468:93–100. http://dx.doi.org/10.1016/S0014-5793(00)01196-0.
36. Hooper JD, Clements JA, Quigley JP, Antalis TM. 2001. Type II transmembrane serine proteases. Insights into an emerging class of cell surface proteolytic enzymes. J. Biol. Chem. 276:857–860. http://dx.doi.org/10.1074/jbc.R000020200.
37. Antalis TM, Buzza MS, Hodge KM, Hooper JD, Netzel-Arnett S. 2010. The cutting edge: membrane-anchored serine protease activities in the pericellular microenvironment. Biochem. J. 428:325–346. http://dx.doi.org/10.1042/BJ20100046.
38. Bugge TH, Antalis TM, Wu Q. 2009. Type II transmembrane serine proteases. J. Biol. Chem. 284:23177–23181. http://dx.doi.org/10.1074/jbc.R109.021006.
39. Donaldson SH, Hirsh A, Li DC, Holloway G, Chao J, Boucher RC, Gabriel SE. 2002. Regulation of the epithelial sodium channel by serine proteases in human airways. J. Biol. Chem. 277:8338–8345. http://dx.doi.org/10.1074/jbc.M105044200.
40. Antalis TM, Bugge TH, Wu Q. 2011. Membrane-anchored serine proteases in health and disease. Prog. Mol. Biol. Transl. Sci. 99:1–50. http://dx.doi.org/10.1016/B978-0-12-385504-6.00001-4.
41. Hatesuer B, Bertram S, Mehnert N, Bahgat MM, Nelson PS, Pöhlman S, Schughart K. 2013. Tmprss2 is essential for influenza H1N1 virus pathogenesis in mice. PLoS Pathog. 9:e1003774. http://dx.doi.org/10.1371/journal.ppat.1003774.
42. Shulla A, Heald-Sargent T, Subramanya G, Zhao J, Perlman S, Gallagher T. 2011. A transmembrane serine protease is linked to the severe acute respiratory syndrome coronavirus receptor and activates virus entry. J. Virol. 85:873–882. http://dx.doi.org/10.1128/JVI.02062-10.
43. Glowacka I, Bertram S, Muller MA, Allen P, Soilleux E, Pfefferle S, Steffen I, Tsegaye TS, He Y, Gnirss K, Niemeyer D, Schneider H, Drosten C, Pohlmann S. 2011. Evidence that TMPRSS2 activates the severe acute respiratory syndrome coronavirus spike protein for membrane fusion and reduces viral control by the humoral immune response. J. Virol. 85:4122–4134. http://dx.doi.org/10.1128/JVI.02232-10.
44. Bertram S, Glowacka I, Muller MA, Lavender H, Gnirss K, Nehlmeier I, Niemeyer D, He Y, Simmons G, Drosten C, Soilleux EJ, Jahn O, Steffen I, Pohlmann S. 2011. Cleavage and activation of the severe acute respiratory syndrome coronavirus spike protein by human airway trypsin-like protease. J. Virol. 85:13363–13372. http://dx.doi.org/10.1128/JVI.05300-11.

Downloaded from http://jvi.asm.org/ on May 4, 2014 by Kyosuke Nagata